Material Molten Time and its Effect on Material Deposition during Electron Beam Selective Melting

C. Guo[1, 2, 3], W. J. Ge[1, 2, 3] and F. Lin[1, 2, 3]

1. Department of Mechanical Engineering, Tsinghua University, Beijing 100084;
2. Key Laboratory for Advanced Materials Processing Technology, Ministry of Education of China, Tsinghua University, Beijing 100084;
3. Biomanufacturing and Rapid Forming Technology Key Laboratory of Beijing, Tsinghua University, Beijing 100084.

REVIEWED

Abstract

Electron Beam Selective Melting (EBSM) is an additive manufacturing technology that directly fabricates parts from metal powders in a layer-by-layer fashion. The material molten time, which equals the total time that material keeps molten during scanning, is selected as an indicator for evaluating the effects of process parameters on material deposition. A finite elements model was established to simulate the molten time distribution within the scanning area for various parameters. Samples were fabricated using the same parameters in simulation. It's found that there is a strong relation between the molten time and material deposition behavior. Appropriate material molten time results in a dense and flat surface. Too little material molten time leads to a non-dense surface and internal pores, and too much material molten time leads to a distorted surface and coarsened microstructures. The material molten time increases with the increase of beam current and with the decrease of scanning velocity and length of scanning line. An optimized process which aims to obtain appropriate and homogeneous molten time within the scanning area is also developed to improve the deposition quality.

1. Introduction

As an additive manufacturing technique for building fully dense metal parts, Electron Beam Selective Melting (EBSM) was attracting more and more attentions in recent years. Similar to the Selective Laser Melting (SLM) process, an electron beam, instead of a laser beam, is used to scan the cross-section of a layer on the surface of a power bed, rapidly melts the metal powder, and deposits the material on the substrate or the previous layers. Fig. 1 is a typical layout of the EBSM system. After the previous layer is scanned, the building platform moves down by an amount equal to the layer thickness, and a new powder layer is spread onto the previous layer. The part is fabricated layer by layer until finished.

Although the EBSM process is similar to SLM, the EBSM process has some unique characteristics. First, the electron beam power density is higher and almost all the electron beam energy is absorbed by the metal materials, resulting in a melted pool with higher temperature and higher penetration depth. Therefore, the EBSM process is suitable for manufacturing fully dense parts with high melting point metal powder, such as Ti-6Al-4V. Second, in order to avoid the collapse of the lowly conductive powder bed, the electron beam

preheats the power bed before melting the cross-section. The preheating step plays a role as the heat treatment, efficiently reduce the thermal stress during fabrication and decrease the brittleness of the fabricated parts. Currently, the EBSM process has been successfully applied to the manufacturing of various materials, including 316L stainless steel, Ti alloy, Co-based alloy, Ni-based superalloy, TiAl superalloy [1-5].

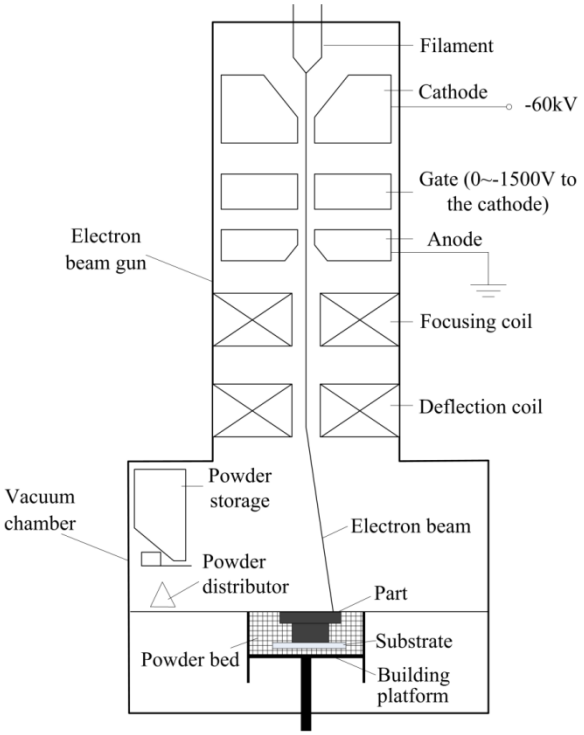

Fig. 1. A typical EBSM system layout

Although the EBSM has many advantages over the conventional means, some defects such as internal pores and uneven surfaces, still exist in the parts built by EBSM. Hence, it is necessary to gather more insight to the thermal phenomena so as to optimize the process. During the EBSM process, the electron beam generally adopts the alternating scan vectors shown in Fig. 2. The temperature fields and temperature histories during the scan provide important information for evaluating the process quality and predicting the microstructures and mechanical properties of the parts. Some numerical models of EBSM were established to simulate the temperature field. Zäh and Lutzmann developed a thermal model to study the effects of beam powder and scanning velocity on the molten pool geometry [6]. In the model developed by Shen and Chou, the temperature-dependent properties of the powder material and the material state change during scanning were taken into consideration, enhancing the modeling accuracy [7]. However, only single scanning track was simulated in the previous research and the relationships between the simulation and experiments still need further study.

Fig. 2. The alternating scan vectors

In this paper, the temperature histories of Ti-6Al-4V during scanning are investigated through a numerical model and Ti-6Al-4V samples are fabricated on an EBSM machine. The material molten time, which equals the total time that material keeps molten during scanning, is selected as an indicator for evaluating the effects of process parameters on material deposition. Effects of the beam current, beam scanning velocity and the length of scanning line on the molten time are studied and a novel process with variable beam current during scanning is proposed to improve the deposition quality.

2. Materials and Methods

2.1. Simulation

The molten flow during the process is neglected, thus the governing equation of the heat transportation is:

$$\frac{\partial H}{\partial t} = \nabla \cdot \lambda \nabla T + S \tag{1}$$

where H is the volumetric enthalpy, λ is the heat conductivity dependent on the phase and temperature, and S is the volume heat source terms. Similar to the laser, the electron beam is typically modeled as a moving heat source with a conical shape and a Gaussian distributed intensity at each depth level. The intensity distribution formula can be seen in Literature [8].

Here are 3 material properties involved in this study: the solid bulk 316L stainless steel, solid bulk Ti-6Al-4V and the Ti-6Al-4V powder. The thermo-physical properties of bulk 316L stainless steel and Ti-6Al-4V are from Literature [9-11]. The volumetric enthalpy of the Ti-6Al-4V powder is considered the same as those of the solid material, and the conductivity is assumed at a very low value 0.2 W/mK. The state change of the power during the process is taken into account in this study. Once the temperature of the powder exceeds the solidus temperature (1900 K), the powder becomes solid and its thermo-physical properties irreversibly change to the same as those of solid Ti-6Al-4V.

A three-dimensional Finite Element model was developed in ANSYS to simulate the temperature histories during the scan. As shown in Fig. 3, the model consists of a solid 316L stainless steel and a thin layer of Ti-6Al-4V powder. Because the process is in the vacuum, the convection between the substrate/powder and surroundings was ignored, and only the radiation was considered. The emissivity of the powder surfaces was assumed at 0.7 [12-13]. The substrate and powder layer were assigned with an initial temperature of 1033 K. The electron acceleration voltage was assigned as 60 kV, the beam diameter 0.6 mm, the beam penetration depth 1 mm, the absorption efficiency 0.9, the powder layer thickness 0.1mm, and the scanning line spacing 0.2 mm.

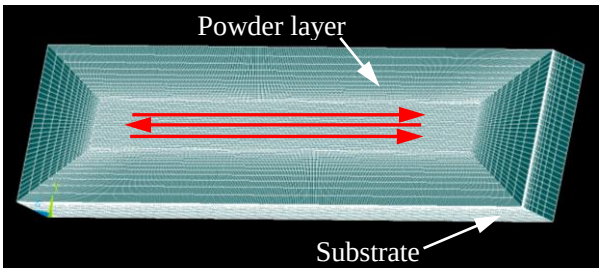

Fig. 3. Finite element model

Scanning parameters such as the scanning velocity, beam current and the length of scanning line were input to the model to investigate their influences on the temperature histories. 6 sets of parameters (A~F) as listed in Table 1 were run in simulation.

Table 1. Scanning parameters used in this study

	A	B	C	D	E	F
Scanning velocity, *v* (mm/s)	500	500	500	250	500	500
Beam current, *I* (mA)	4	8	12	6	10	10
Length of scanning line, *L* (mm)	20	20	20	20	20	10

2.2. Experiments

The Ti-6Al-4V powder used in this study was spherical with a particle size between 15 and 150 μm, and the average particle size was 80 μm. Samples were built on a self-developed EBSM machine, which was equipped with an electron gun with an accelerating voltage of 60 kV and a maximum beam current of 50 mA.

6 samples (numbered A~F) were fabricated. A 316L stainless steel substrate with a size of $90 \times 90 \times 10$ mm^3 was placed on the powder bed. Before depositing, the electron beam scanned the starting plate for 20 minutes with a beam current of 15 mA, a defocusing current of 150 mA, a scanning line spacing of 1 mm and a scanning velocity of 10 m/s. The layer thickness was 0.1 mm. For each powder layer, the process included two steps: preheating and melting. The preheating step was aimed to maintain a high temperature in the powder bed, so as to avoid the collapse of the powder bed. In this step the electron beam only slightly sintered the powder, and thus had a limited impact on the material deposition of the layers. For all samples, scanning parameters during the preheating step were fixed. In contrast, scanning parameters during the melting step had a critical impact on the material deposition of the layers. The scanning parameters for sample A~F were the same as the parameters used in the simulation (see in Table 1). For each sample, about 30 layers were deposited.

Results of the simulation and the fabricated samples were analyzed and compared, establishing a linkage between the material molten time and material deposition.

3. Results and Discussions

3.1. Material Molten Time vs. Material Deposition

For the parameter set A~C, the temperature histories at the middle point of the scanning area was plotted in Fig. 4. As the scanning line spacing (0.2mm) is smaller than the beam radius (0.3 mm), the material is melted by the electron beam for several times. With the increase of the beam current, the peak temperature of the material increases. In order to better illustrate the relationship between the temperature histories and material deposition, the material molten time, which equals the total time that the material keeps melted, is introduced. For example, the time that the temperature is above the melting point (1920 K) for parameter set A~C is 14.4, 41.2, and 127.2 ms, respectively. It is obvious that the molten time increases with the increase of energy input.

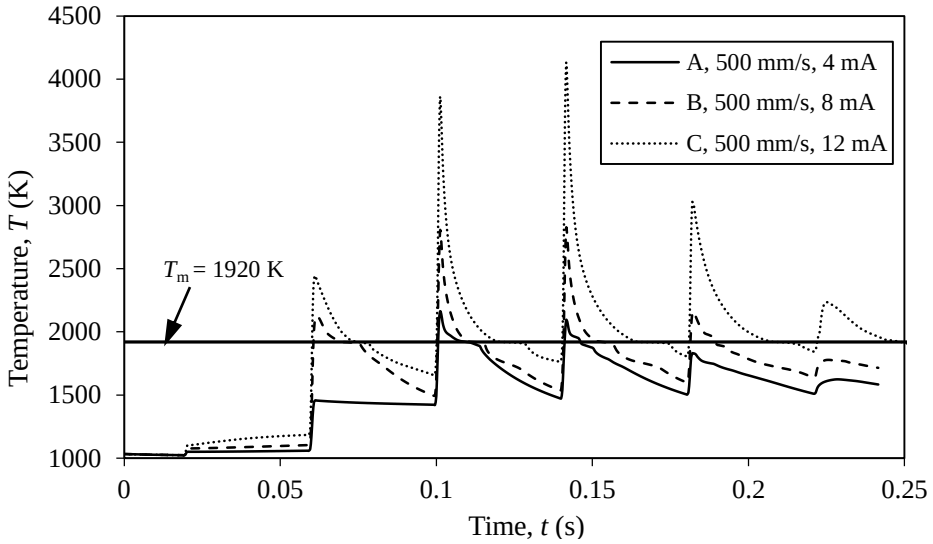

Fig. 4. Material temperature histories for parameter set A~C

The material molten time along the center line parallel to the scanning direction is plotted in Fig. 5. The corresponding sample A~C were analyzed in terms of the top surface topography and internal microstructures. With the molten time at a low level, the top surface of sample A is non-dense with agglomerates, and many internal pores exist. As the molten time increases, the surface of sample B becomes dense free of agglomerates. The surface slightly concaves at the middle yet is basically flat. The sample is highly dense and basket-weave microstructures consisting fine acicular α-phase grains surrounded by interfacial β-phase can be observed in most of the section. However, with too much molten time, the surface of sample C is significantly distorted and the α/β phases in most of the section also coarsen.

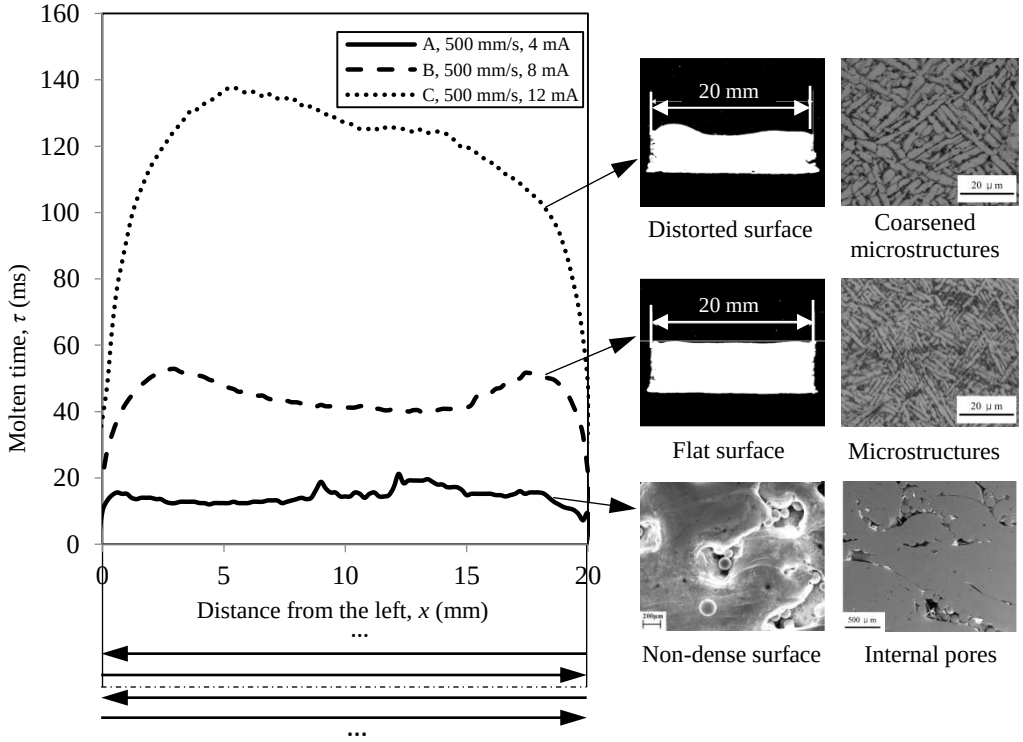

Fig. 5. Material molten time and material deposition

There is a strong relation between the material molten time and material deposition. The material molten time reflects the amount and lifetime of the liquid metal phase during scanning and can be considered as a key issue predicting the material deposition. If the molten time is little, due to the lack of wetting capacity of molten pool on the substrate or previous layers, the scanning track tends to break up in to balls as a result of the surface tension. An increase in the molten time represents a larger amount and a longer lifetime of the liquid phase. The liquid has sufficient time to flow and spread before solidifying, filling in the pores and leading to a dense surface. However, here exist two issues affecting the surface shape. First, due to the alternating scan vectors, the peak values of molten time appear at both ends of the center line. The liquid metal at both the ends is more than that at the middle, thus the metal liquid attaches to the larger molten pool, resulting in a distorted surface. Second, under the interaction of vapour pressure and surface tension, the liquid metal flows in the direction opposite to the electron beam scanning. This phenomenon has also been observed in the electron beam surfi-sculpt process [14]. In the alternating scanning, the liquid metal flows outside from the middle, leading to a distorted surface. If the molten time is in an appropriate range, the influences of the above two issues is negligible, thus the sample surface is basically flat. Nevertheless, the influences of the above two issues grows with the increase of the molten time. If the amount and lifetime of the liquid phase are too large, the liquid metal tends to alter its shape into a distorted one before solidifying. In addition, with too much molten time, the primary basket-weave α/β phase coarsens. The fine α phase precipitated in the β phase results in high strength, while the coarsened α lath leads to a lower strength and a better ductility [15].

3.2. Effect of Scanning Velocity

For the parameter set C~E, the material molten time along the center line parallel to the scanning direction is plotted in Fig. 6. The molten time for parameter C is significantly higher than that for parameter D and E. Correspondingly, the sample C has a distorted surface, and the surfaces of sample D and E are basically flat.

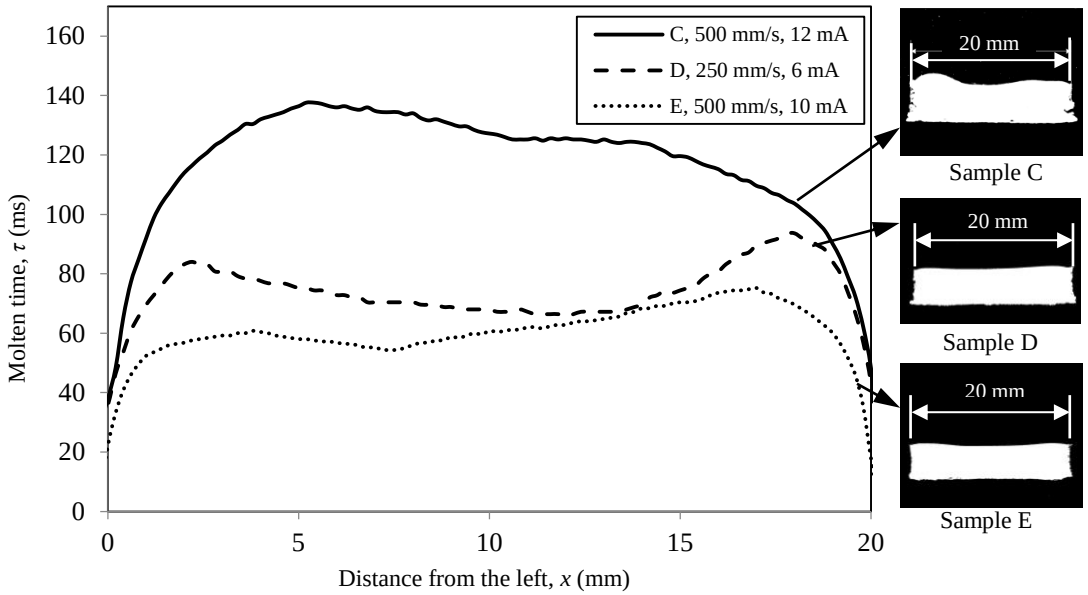

Fig. 6. Effect of scanning velocity on molten time and material deposition

In the SLM process, a combined parameter called energy density is generally used to estimate the effects of the parameters such as beam power *P*, scanning velocity *v*, and scanning line spacing *s*. From Beaman et al., the energy density is described as [16]:

$$\varepsilon = \frac{4P}{\pi v s} \tag{2}$$

The electron beam power *P* equals the product of accelerating voltage *U* and beam current *I*, therefore,

$$\varepsilon = \frac{4UI}{\pi v s} \tag{3}$$

From Eqn. 3, the energy densities of parameter set C and D are equal, yet the surfaces of sample C and D are quite different: sample C is significantly distorted and sample D is flat. The difference between sample C and D can be explained by the molten time. With too much molten time, the surface of sample C becomes distorted. Both the sample D and E have a flat surface because their molten time is comparable. In other words, as the scanning velocity doubles from 250 to 500 mm/s, the beam current should be less than the doubled value (12 mA) to keep the molten time in an appropriate range.

The effect of scanning velocity on molten time can be explained by the thermal cycles during the scan. As the scanning lines overlap, the material undergoes several heating and cooling cycles: it is heated as electron beam approaches, and cools down as the electron beam leaves. An increase in scanning velocity results in a shorter heat interval and a smaller amount of heat loss in the heat interval. As a result, the heat is more concentrated and hence the beam current required to obtain the same molten time is lower than the value determined by Eqn. 3.

3.3. Effect of Length of Scanning Line

For the parameter set E and F, the material molten time along the center line parallel to the scanning direction is plotted in Fig. 7. The molten time of parameter F is significantly higher than that of parameter E. Correspondingly, the sample F has a distorted surface, and the surface of sample E is flat.

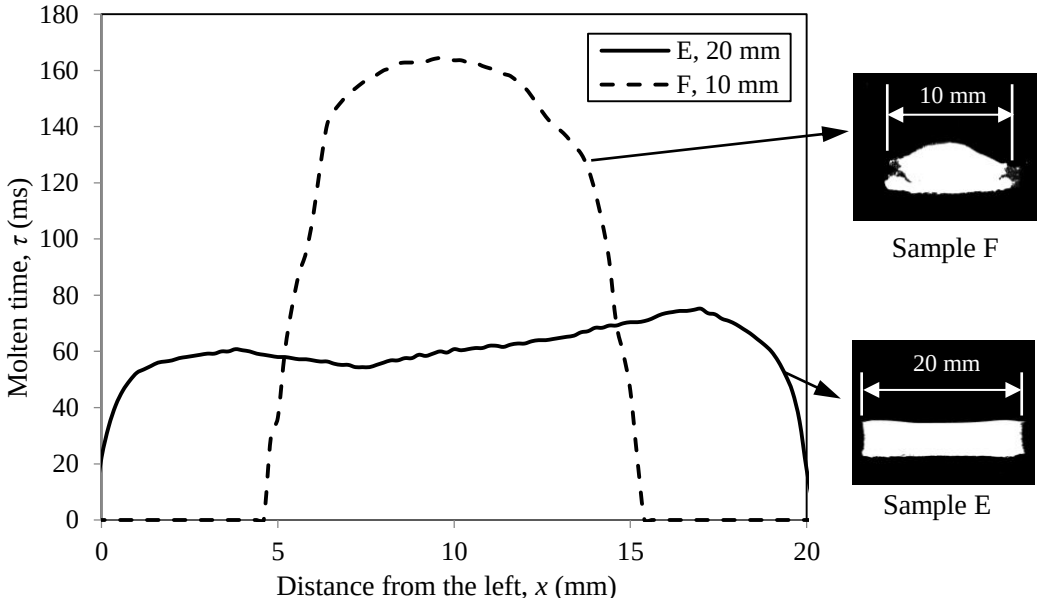

Fig. 7. Effect of length of scanning line on molten time and material deposition

A decrease in the scanning line length leads to an increase in the material molten time. A less scanning line length leads to a shorter heat interval, and thus the material loses less amount of heat before they are heated again by the electron beam, yielding a higher extent of heat concentration, and consequently a larger amount and a longer lifetime of the liquid phase. In other words, as the scanning line shortens, the beam current should be reduced to obtain the same molten time.

4. Process Optimization Method

In order to reduce the risk of surface distortion and obtain uniform microstructures and properties, a process optimization method is proposed. The principle of the process optimization is to (1) keep the material molten time in an appropriate range (60~100 ms in this study) and (2) homogenize the molten time distribution within the scanning area. Fig. 8 is the flow chart of process optimization. For a given scanning velocity, a reference beam current which leads to a dense and flat surface at standard scanning line length can be determined by simulation or experiment. As the scanning line length varies during fabrication, the beam current is adjusted in real time dependent on the length of scanning line. Take the case in Fig. 9 as example, with the increase of scanning line length, the beam current increases logarithmically from 1.4 to 10 mA to homogenize the molten time distribution within the scanning area.

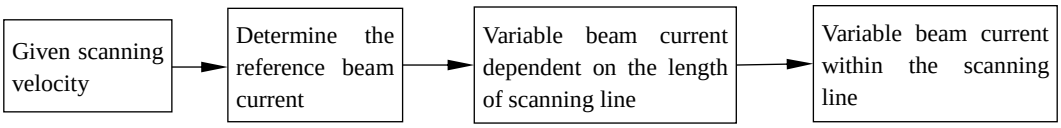

Fig. 8. Flow chart of the process parameters optimization

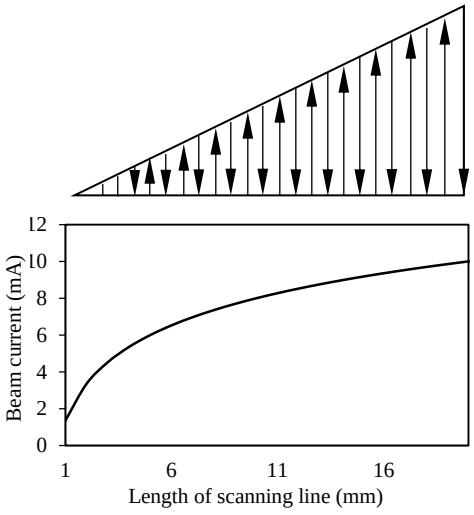

Fig. 9. Variable beam current dependent on the length of scanning line

The beam current can be varied within the scanning line to obtain a more homogeneous molten time distribution. Fig. 10 is a simulation result comparison between constant and variable beam current. The scanning velocity is 250 mm/s and the scanning length is 20 mm. With a constant beam current of 6 mA, the material molten time along the scanning line significantly concave at the middle. With an optimized beam current

distribution (solid line), the material molten time distribution is more homogeneous.

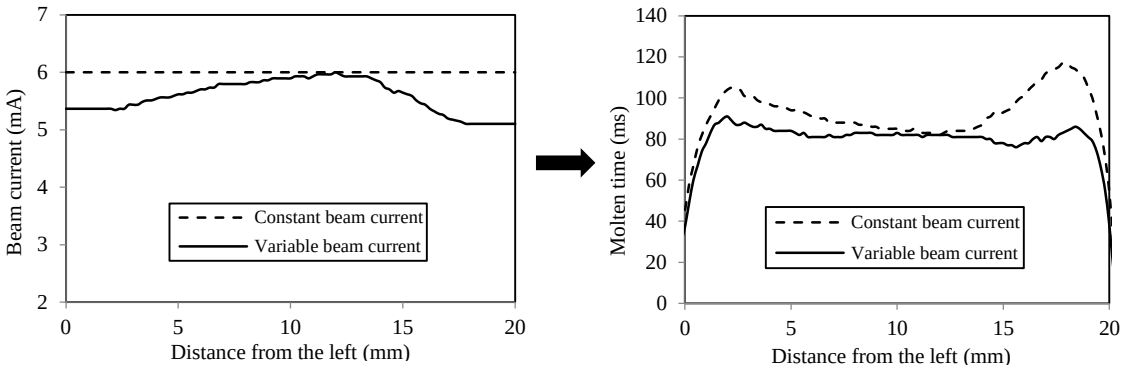

Fig. 10. Simulation result comparison between constant and variable beam current

5. Future work

The numerical model needs to be improved to enhance the simulation accuracy. An average emissivity of the powder layer surface was used in this study. Actually, the powder layer emissivity is dependent on temperature and phase. As the temperature of powder layer increases, the emissivity varies. And as the powder melts to liquid and cools down to solid, its emissivity also changes. The temperature- and phase-dependent emissivity will be taken into consideration in future simulation.

An infrared camera will be used to measure the temperature field and histories during scanning. Then the measuring results will be compared with the simulation results to verify the numerical model and make the simulation more convincing. The camera has a spectral range of 0.8 μm to 1.1 μm wavelength, and has a 640 × 480 uncooled Si-CMOS array. The detectable temperature range is from 400 ℃ up to 2000 ℃. The maximum frame rate of the image capturing system is at 25 Hz.

In additive manufacturing based on powder bed, the laser or beam power and the scanning velocity is generally constant. In this paper, a variable beam current process, which aims to homogenize the molten time distribution within the scanning area, is proposed to improve the fabrication quality. Effects of the optimized process were studied through numerical simulation in this paper and needs further research through experiments in future. This optimized process will be applied to an EBSM system and a comparison of samples built by the constant and variable beam current process will be conducted.

6. Conclusions

1. The material molten time during scanning can be considered as an indicator for evaluating the effects of process parameters on material deposition. Appropriate material molten time results in a dense and flat surface. Too little material molten time leads to a non-dense surface and internal pores, and too much material molten time leads to a distorted surface and coarsened microstructures.

2. The material molten time increases with the increase of beam current and with the decrease of scanning velocity and length of scanning line.

3. Compared to the constant beam current scanning, the variable beam current scanning is an optimized process that homogenizes the molten time distribution within the scanning area.

Acknowledgements

The authors would like to acknowledge the funding of 2013 Beijing Science and Technology Development Project, No. D13110400300000 and D131100003013002.

References

1. Cormier, D., Harrysson, O. L. A., Mahale, T., West II, H. A., 2008, "Freeform Fabrication of Titanium Aluminide via Electron Beam Melting Using Prealloyed and Blended Powders", Advanced Material Science and Engineering, 2007, pp. 6822-6825.
2. Facchini, L., Magalini, E., Robotti, P., Molinari, A., 2009, "Microstructure and mechanical properties of Ti-6Al-4V produced by electron beam melting of pre-alloyed powders", Rapid Prototyping Journal, 15, pp. 171-178.
3. Murr, L. E., Martinez, E., Pan, X. M., Gaytan, S. M., Castro, J. A., Terrazas, C. A., Medina, F., Wicker, R. B., Abbott, D. H., 2013, "Microstructures of Rene 142 nickel-based superalloy fabricated by electron beam melting", Acta Materialia, 61, pp. 4289-4296.
4. Sun, S. H., Koizumi, Y., Kurosu, S., Li, Y. P., Matsumoto, H., Chiba, A., 2014, "Build direction dependence of microstructure and high-temperature tensile property of Co-Cr-Mo alloy fabricated by electron beam melting", Acta Materialia, 64, pp. 154–168.
5. Yan, Y. N., Qi, H. B., Lin, F., He, W., Zhang, H. R., Zhang, R. J., 2007, "Produced three-dimensional metal parts by electron beam selective melting", Chinese Journal Mechanical Engineering, 43, pp. 87-92.
6. Zäh, M. F., and Lutzmann, S., 2010, "Modeling and Simulation of Electron Beam Melting", Production Engineering. Research and Development, 4, pp. 15-23.
7. Shen, N. G., and Chou, K., 2012, "Thermal modeling of Electron Beam Additive Manufacturing Process: Powder Sintering Effects", In Proceedings of the ASME 2012 International Manufacturing Science and Engineering Conference, June 4-8, 2012, Notre Dame, Indiana, United States, pp.1-9.
8. Wang, L., Felicelli, S., Gooroochurn, P. T., Wang, P. T., and Horstemeter, M. F., 2008, "Optimization of the LENS process for steady molten pool size," Materials Science and Engineering A, 474, pp. 148-156.
9. Mills, K. C., Su, Y., Li, Z., and Brooks, R. F., 2004, "Equations for the Calculation of the Thermo-physical Properties of Stainless Steel," ISIJ International, 44(10), pp. 1661-1668.
10. Boivineau, M., Cagran, C., Doytier, D., Eyraud, V., Nadal, M. H., Wilthan, B., and Pottlacher, G., 2006, "Thermophysical Properties of Solid and Liquid Ti-6Al-4V (TA6V) Alloy," International Journal of Thermophysics, 27(2), pp. 507-529.
11. Roberts, I. A., Wang, C. J., Esterlein, R., Stanford, M., and Mynors, D. J., 2009, "A three-dimensional finite element analysis of the temperature field during laser melting of metal powders in additive layer manufacturing," International Journal of Machine Tools

& Manufacture, 49, pp. 916-923.
12. Gonzalez-Fernandez, L., Risueno, E., Perez-Saez, R. B., and Tello, M. J., 2012, “Infrared normal spectral emissivity of Ti – 6Al – 4V alloy in the 500-1150 K temperature range”, Journal of Alloys and Compounds, 541, pp. 144-149.
13. Sih, S. S., and Barlow, J. W., 2004, “The Prediction of the Emissivity and Thermal Conductivity of Powder Beds”, Particulate Science and Technology, 22, pp. 427-440.
14. Wang, X., Gong, S., Guo, E., Zhao, H., and Xu, H., 2012, “Primary study on electron beam surfi-sculpt of Ti-6Al-4V,” Advanced Materials Research, 418-420, pp. 772-776.
15. Chen, B., Shao, B., Liu, D., Tian, X., Liu, C., and Wang, H., 2014, “Effect of heat treatment on microstructures and mechanical properties of Laser Melting Deposited TC17 titanium alloy”, Chinese Journal of Lasers, 41, pp. 1-7.
16. Beaman, J. J., Barlow, J. W., Bourell, D. L., Crawford, R. H., Marcus, H. L., McAlea, K. P., 1997, “Solid Freeform Fabrication: A new direction in Manufacturing”, Kluwer Academic Publisher, Massachusetts, pp. 205-207.